Electric Drives with Wide Bandgap Devices for Two-Phase Very Low Inductance Machines

Yibin Zhang, *Student Member, IEEE*, Damien Lawhorn, *Student Member, IEEE*, Peng Han, *Member, IEEE*, Aaron M. Cramer, *Senior Member, IEEE*, and Dan M. Ionel, *Fellow, IEEE*
SPARK and SCOPE Labs, ECE Dept., University of Kentucky, Lexington, KY, USA
yibin.zhang@uky.edu, damien.lawhorn@uky.edu, peng.han@uky.edu, aaron.cramer@uky.edu, dan.ionel@ieee.org

***Abstract*—Slotless and coreless machines with low inductance and low core losses are attractive for high speed and high power density applications. With the increase in fundamental frequency, typical drive implementations using conventional silicon-based devices are performance limited and also produce large current and torque ripples. This paper presents a systematic study of proposed drive configurations implemented with wide bandgap (WBG) devices in order to mitigate such issues for 2-phase very low inductance machines. Two inverter topologies, i.e., a dual H-bridge inverter with maximum redundancy and survivability and a 3-leg inverter for reduced cost, are considered. Feasible modulation schemes are derived based on theoretical analysis and the associated maximum output voltages are identified. Simulation and experimental results are provided to validate the feasibility of drive systems and the effectiveness of analysis.**

***Index Terms*—Axial flux permanent magnet machines, coreless machines, electric drives, operating range, two-phase, very low inductance machines, wide bandgap.**

I. Introduction

Low inductance machines have shown attractiveness for various applications, especially where high speed operation is required [1], [2]. However, with pulse width modulation (PWM) inverters, low inductance machines typically show visible switching reflected current harmonics. Though the dc bus utilization is improved at high speed, PWM voltage produces considerable harmonics in machine currents, degrading the efficiency and reliability of drive systems [3].

In conventional drive systems for low inductance machines, filters, such as LC and LCL filters have to be implemented to reduce PWM reflected current harmonics [4]. LC filters do not contain any resistive components, so the voltage/current waveform distortion appears especially in LC resonant area, and leads to circulating currents between the inverter and the filter [5]. Active damping compensation and LCL filters have been proposed to address the aforementioned issues. However, the cost, weight, and volume added by the filters still need to be reduced.

Wide band-gap (WBG) semiconductor devices, such as SiC MOSFETs, enable the PWM frequency capability of 50 to 100 kHz or even higher, which keeps the current ripple within acceptable limits for low inductance machine drives [6]. WBG semiconductors outperform silicon counterparts in terms of on-resistance. Employing one H-bridge for each phase is the most common drive topology which offers the highest per-phase dc bus utilization but at the same time the highest number of devices and cost [7]. Additionally, the increase of the switching speed in power devices increases the power density of power electronic converters as it reduces the weight and volume of passive components [8].

To further improve the compactness, reduce low cost, and enhance the robustness, single-phase and two-phase machines have been increasingly drawing attention [9]. Single-phase and two-phase motors work well in constant-speed applications but show difficulties when variable-speed performance is needed [10]. To improve the variable-speed capability of 2-phase machines, it becomes necessary to explore alternative inverter topologies and associated modulation schemes and the optimal use of WBG devices in 2-phase machine drives [11], [12].

In this paper, two drive configurations (in Fig. 1) for two-phase low inductance machines are studied in terms of the operating capability, survivability, and cost. For the proposed dual H-bridge drive topology, each phase is electrically isolated and driven by one H-bridge and a separate dc supply. In the case of failure in one phase, the other phase is still capable of supplying the motor. However, the dual-topology consists of a large number of switching devices, two capacitors with high capacitances, and multiple supplies, which may increase the system cost. A 3-leg topology as a cost-effective solution is proposed and studied. A noticeable limitation of 3-leg inverters in driving two-phase motors is that the root mean square (RMS) value of the common leg current is higher than those of the other two legs that necessitates the utilization of switches with higher current ratings at least in one leg. The low inductance machines under study are coreless axial-flux permanent-magnet (AFPM) machines comprised of multiple rotors and stators with Litz wire or printed circuit board windings. And the two phases of the coreless AFPM machine are electrically and magnetically isolated.

II. Modulation for Dual H-Bridge Inverter

The first topology, referred to as the dual H-bridge inverter, consists of two independent H-bridges and two separate dc sources, as illustrated in Fig. 1a. Each phase winding of the two-phase machine is supplied by a single H-bridge, which provides full electrical isolation between two phases. The two phase windings are also magnetically isolated since they are designed to have a displacement of 90 electrical degrees. This drive configuration is expected to have the maximum reliability considering the inherent electrical and magnetic isolation between two phases.

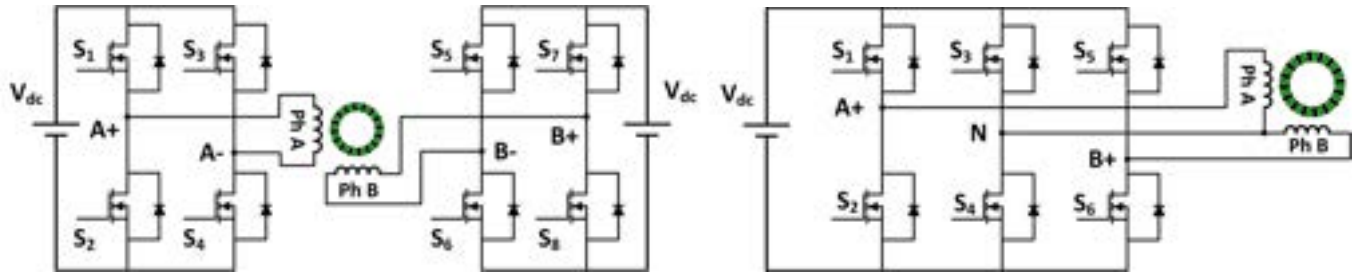

(a) (b)

Fig. 1. Proposed inverter topologies for two-phase very low inductance machines considered in the study: (a) two H-bridges supplied by two separate dc sources, (b) a three-leg inverter with one leg shared by two phases, which has a cost advantage of 1/4 fewer switches and one dc supply.

To drive the two-phase machine with the dual H-bridge inverter topology, suitable modulation schemes have to be derived. To produce the rotating magnetic field required for torque production, the fundamental components of the inverter output voltages are required to have the same amplitude and a phase shift of 90 electrical degrees. Assuming the amplitude of the inverter output voltage is V, the fundamental components of the two phase voltages for the dual H-bridge inverter are:

$$\begin{cases} V_{PhA} & = V_{A^+O} - V_{A^-O} \\ & = m\left(\frac{V_{dc}}{2}\right)\cos(\omega t - \varphi), \\ V_{PhB} & = V_{B^+O} - V_{B^-O} \\ & = m\left(\frac{V_{dc}}{2}\right)\cos(\omega t - \varphi - \pi/2), \end{cases} \tag{1}$$

where V_{PhA} and V_{PhB} are the terminal voltages of Phase A and Phase B windings, respectively. O is the middle point of the dc bus. V_{A^+O} and V_{B^+O} represent the voltage of A^+ and B^+ to O, respectively. m and V_{dc} are the modulation index and dc voltage amplitude, respectively. The angular frequency of the two-phase machine ω is obtained from $\omega = 2\pi f$, and φ is the initial phase of the reference wave. Equation (1) indicates the carrier-based sinusoidal PWM (SPWM) scheme can be used for the dual H-bridge inverter.

III. Modulation for Dual 3-Leg Inverter

The second topology is a 3-leg inverter (Fig. 1b). Each phase winding of the machine is supplied by one H-bridge but one leg is shared by two phases. This change reduces the number of required WBG devices by 1/4 and is more attractive in terms of the system cost. Compared with the dual H-bridge, the 3-leg topology is more susceptible to failures of power supply, in which case both phase windings are out of power and fault-tolerant operation becomes impossible.

The fundamental components of the two phase voltages for the 3-leg inverter are similar to those expressed by equation (1) except that "A^-" and "B^-" are replaced by N:

$$\begin{cases} V_{PhA} & = V_{A+O} - V_{NO} \\ & = m\left(\frac{V_{dc}}{2}\right)\cos(\omega t - \varphi), \\ V_{PhB} & = V_{B+O} - V_{NO} \\ & = m\left(\frac{V_{dc}}{2}\right)\cos(\omega t - \varphi - \pi/2). \end{cases} \tag{2}$$

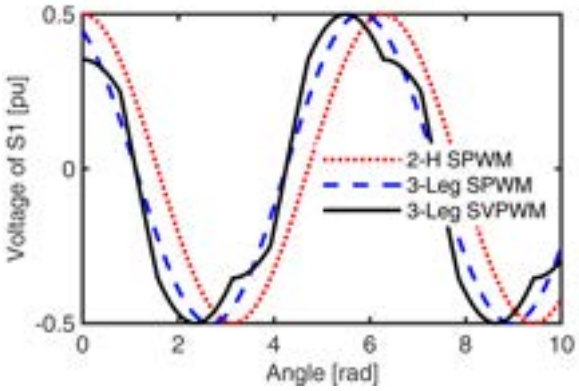

Fig. 2. Reference signals of the two inverter topologies with various modulation schemes (full modulation).

The solution that can achieve the maximum reference amplitude is:

$$\begin{cases} V_{A^+O} & = m\left(\frac{V_{dc}}{2}\right)\left[\frac{2}{3}\cos(\omega t) - \frac{1}{3}\sin(\omega t)\right], \\ V_{NO} & = m\left(\frac{V_{dc}}{2}\right)\left[-\frac{1}{3}\cos(\omega t) - \frac{1}{3}\sin(\omega t)\right], \\ V_{B+O} & = m\left(\frac{V_{dc}}{2}\right)\left[-\frac{1}{3}\cos(\omega t) + \frac{2}{3}\sin(\omega t)\right]. \end{cases} \tag{3}$$

Equation (3) indicates both the carrier-based SPWM and space vector PWM (SVPWM) can be used for the 3-leg inverter. In the case of SVPWM, the phase voltage is not symmetrical due to the unbalance in V_{A^+O}, V_N and V_{B^+O}, as shown in Fig. 2.

IV. The Operating Range Analysis and Simulation

A physical phase variable model of the two-phase coreless AFPM machine is developed, whose PM flux linkage and phase inductance are extracted from 3-dimensional finite element analysis (FEA). It has been shown that coreless designs usually have very low inductance and the selection of switching frequency plays an important role in improving the system performance [13].

The operating range is first analyzed for the two proposed configurations (shown in Fig. 3). The simulation results for the two inverters with various modulation schemes are presented in Fig. 4. And the simulation results of phase currents are shown in Fig. 5.

The two-phase motor is operated at 266.67Hz fundamental frequency with full load. The phase currents I_a and I_b for the

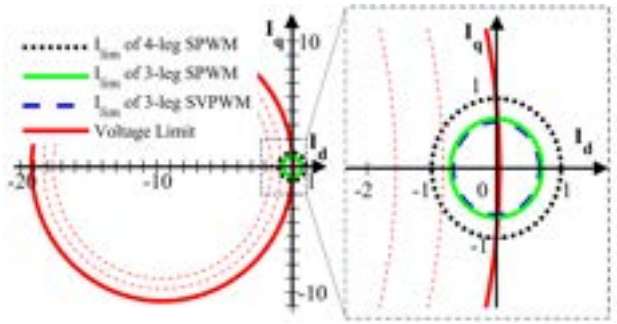

Fig. 3. The operating ranges of the proposed two drive systems with different modulation schemes (in p.u.).

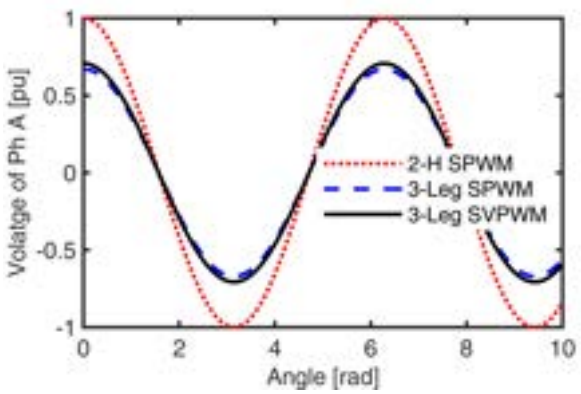

Fig. 4. Phase A voltage. Compared with 1.0 pu voltage rating of the dual H-bridge topology with SPWM, the 3-leg topology with SPWM and SVPWM can at most produce 0.67 pu and 0.71 pu voltage, respectively, under the same condition.

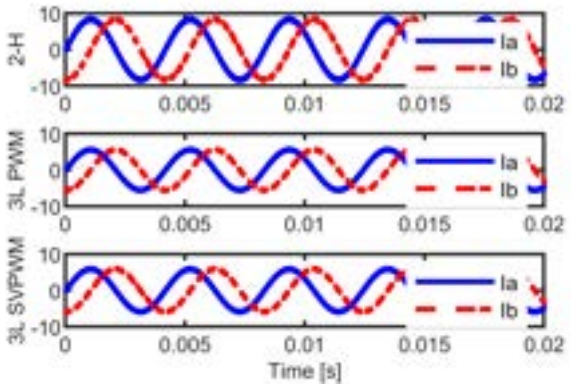

(a)

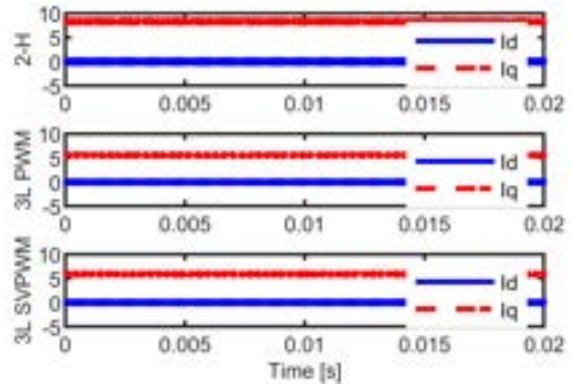

(b)

Fig. 5. Simulated performance of the two drive configurations with various modulation schemes, (a) ab phase currents, (b) dq currents. To have the same current/torque capability for the 3-leg drive system, a higher V_{dc} is necessary, and hence higher voltage ratings for the WBG devices, are required.

3-leg drive systems with PWM and SVPWM are 71% and 67% of dual H-bridge system capacity under the same condition (in Fig. 5a). The dq currents I_d and I_q for the dual H-bridge drive system are 0 and 8.30A, respectively. With the same dc bus voltage, the I_q of the 3-leg drive system is reduced to 5.56A with SPWM and 5.87A with SVPWM, respectively, as shown in Fig. 5b. To have the same current/torque capability, it is necessary to increase the V_{dc} for the 3-leg drive system.

To apply the two-phase very low inductance machine for variable speed applications, the closed-loop speed control based on i_d = 0 control strategy was implemented, as illustrated by the schematic diagram in Fig. 6a. Responses of motor speed and phase currents to a step change in the reference speed are presented in Fig. 6b. At 0.1s, the speed is increased from 1,000 r/min to 1,500 r/min, and frequency of phase currents i_a and i_b is increased accordingly.

V. Experimental Validation

An experimental test setup has been built to validate the theoretical analysis and evaluate the performance of the studied drive systems. The motor to be tested is a two-phase coreless AFPM machine with two surface-mounted PM rotors and a central PCB stator, whose exploded view is shown in Fig. 7a. The PCB stator has two independent phase winding stacks with 90 electrical degrees of angular displacement between each other. Each phase stack consists of 6 PCB layers and multiple traces per layer. The developed test fixture is shown in Fig. 7b, which can be used to adjust the airgap length during the test. The parameters of the designed machine and drive system are listed in TABLE I.

The drive systems using WBG devices and the dSPACE control board are built as shown in Fig. 8. Two isolated

TABLE I
Parameters of The Developed Motor and Drive Prototype.

Number of poles p	32
Open-circuit PM fluxlinkage λ_m	0.087 Wb
Inertia of rotor J	0.0421 kg.m^2
Phase inductance L_s	188.8 uH
Phase resistance r_s	0.566 Ω
Fundamental frequency f	266.67 Hz
Rated torque T	7.1 Nm
Rated speed ω_n	1,000 r/min
Rated current I_n	3.45 A
Rated power P_{rated}	1 hp
dc bus voltage V_{dc}	300 V
Switching frequency f_w	10 kHz

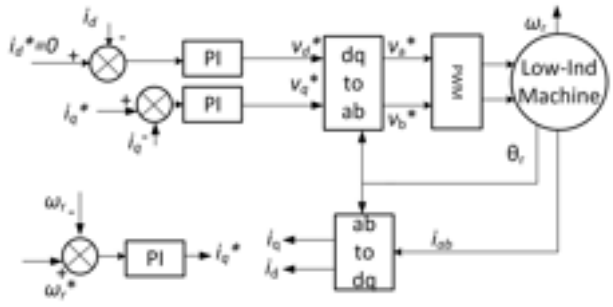

(a)

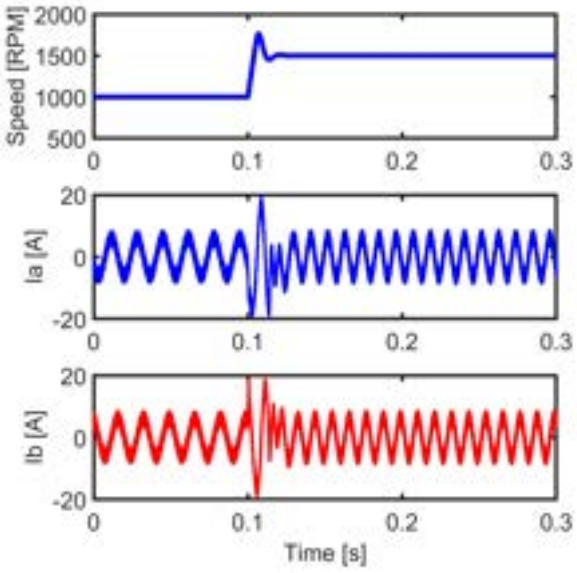

(b)

Fig. 6. Closed-loop speed control, (a) control strategy for the two-phase very low inductance machine drive systems, (b) speed and phase currents when speed is increased from 1,000 r/min to 1,500 r/min at 0.1s of simulation time.

dc supplies with separate dc capacitors feed the two phase windings independently. The dSPACE control board generates gating signals to drive the inverters. Based on the proposed modulation schemes, gating signals for the two phases are generated 90 electrical degrees apart from each other, matching the machine drive requirements. CREE SiC MOSFET power semiconductors C2M0280120D (rated at 1200V/10A and operated at switching frequency 10kHz and 100kHz) are employed for the prototype drive system.

The experimental results are presented in Fig. 9. It can be seen that with the increase of switching frequency enabled by SiC devices (from 10kHz to 100kHz), the current ripple reduces significantly in each set of results. With the same dc bus voltage and modulation index, the dual H-bridge drive system can produce the maximum phase currents (2.64A), while the 3-leg drive systems can only produce 1.87A with SVPWM and 1.77A with SPWM, respectively. To have the same operating range, it is necessary to increase the dc bus voltage for the 3-leg topology.

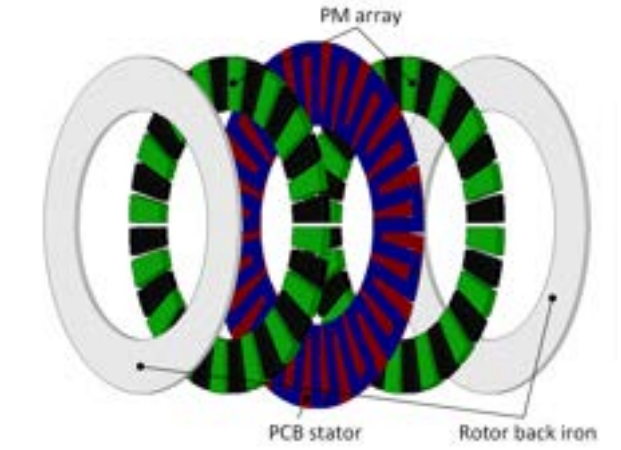

(a)

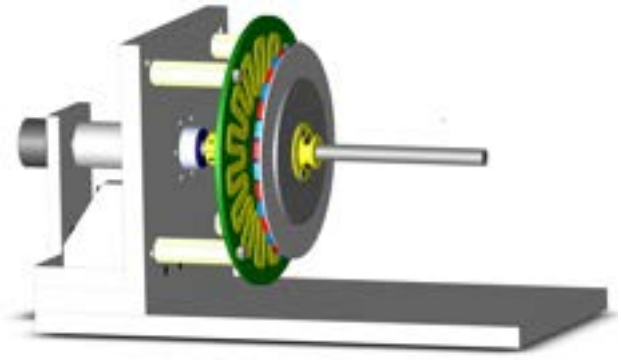

(b)

Fig. 7. Motor prototyping and testing, (a) exploded view of coreless prototype with PCB stator windings, (b) test fixture with motor installed. The developed fixture is capable of testing AFPM machines with various airgap lengths.

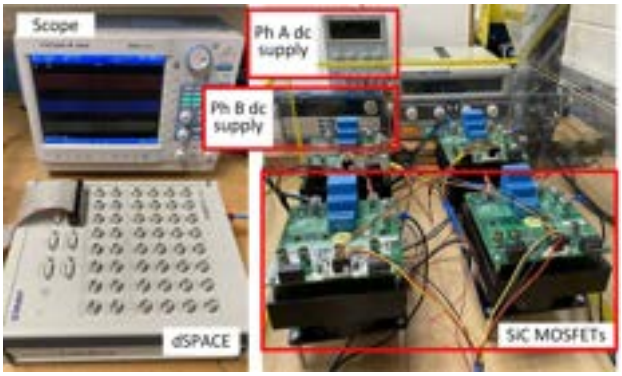

Fig. 8. Motor drive prototypes with SiC MOSFETs and dSPACE control board.

VI. Conclusion

This paper evaluates the performance a dual H-bridge and a 3-leg inverter based drive system for two-phase coreless AFPM machines featuring very low inductance. It is shown that the dual H-bridge inverter supplied by two separate dc sources provides complete electrical isolation between phases. If one supply fails, a single phase may still be supplied and thus the dual H-bridge has maximum survivability.

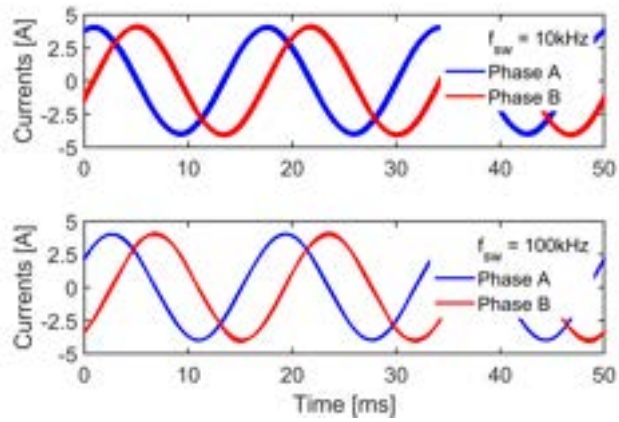

(a)

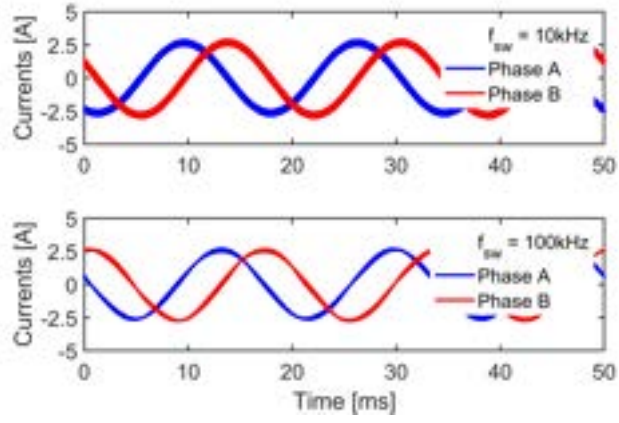

(b)

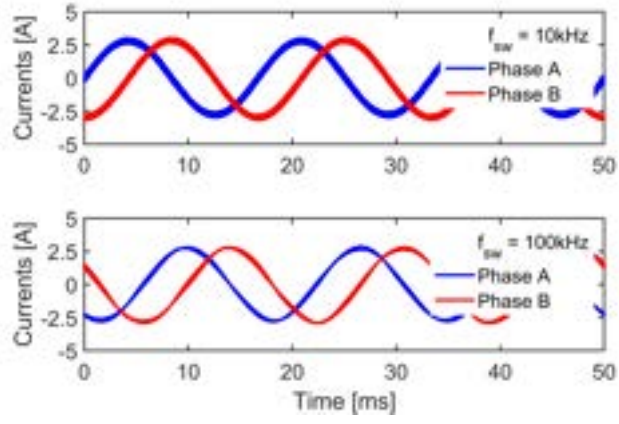

(c)

Fig. 9. Experimental results of the proposed two inverter topologies with suitable modulation schemes, (a) dual H-bridge inverters with SPWM, (b) three-leg inverter with SPWM, (c) three-leg inverter with SVPWM. By using WBG devices, the switching frequency can be significantly increased, which helps reduce the current ripple and thus torque ripple.

In contrast, with respect to output capability, the 3-leg drive system can produce at most 71% the voltage generated by the dual H-bridge inverter for the same dc bus voltage. In the case of a supply failure, the whole system of the 3-leg inverter fails. In the 3-leg topology there is only one dc source and one of the three legs is shared by two phases. Therefore, this configuration offers a more cost effective solution by reducing power semiconductor switch count from 8 to 6, and reducing dc supply count from 2 to 1, compared with the dual H-bridge configuration at the same dc bus rating.

It is also experimentally shown that the current ripple is effectively reduced by implementing the two drives with WBG devices and operating the inverters at high switching frequencies. The 100kHz switching frequency enabled by SiC devices, compared to the 10kHz achievable by traditional silicon devices, largely reduces the current ripple and total harmonic distortion.

ACKNOWLEDGMENT

The support of National Science Foundation NSF Grant #1809876, of University of Kentucky, and of the L. Stanley Pigman endowment, Inc. is gratefully acknowledged.

REFERENCES

[1] M. Leandro, N. Bianchi, M. Molinas, and R. B. Ummaneni, "Low inductance effects on electric drives using slotless permanent magnet motors: A framework for performance analysis," in *Proc. IEEE Int. Electr. Mach. Drives Conf. (IEMDC)*, 2019, pp. 1099–1105.

[2] V. Rallabandi, N. Taran, D. M. Ionel, and J. F. Eastham, "Coreless multidisc axial flux pm machine with carbon nanotube windings," *IEEE Trans. Magn.*, vol. 53, no. 6, pp. 1–4, 2017.

[3] M. S. Islam, R. Mikail, and I. Husain, "Extended field weakening range in slotless/coreless permanent magnet machines," in *Proc. IEEE Energy Convers. Congr. and Expo. (ECCE)*, 2019, pp. 1769–1775.

[4] C. Hsu, S. Yang, and J. Chen, "Implementation of low inductance permanent magnet machine drive with LC filter for field oriented control," in *Proc. IEEE Energy Convers. Congr. and Expo. (ECCE)*, 2019, pp. 6140–6146.

[5] J. He and Y. W. Li, "Generalized closed-loop control schemes with embedded virtual impedances for voltage source converters with lc or lcl filters," *IEEE Trans. Power Electron.*, vol. 27, no. 4, pp. 1850–1861, 2012.

[6] T. P. Chow, I. Omura, M. Higashiwaki, H. Kawarada, and V. Pala, "Smart power devices and ics using gaas and wide and extreme bandgap semiconductors," *IEEE Trans. Electron. Dev.*, vol. 64, no. 3, pp. 856–873, 2017.

[7] M. T. Bartholet, T. Nussbaumer, and J. W. Kolar, "Comparison of voltage-source inverter topologies for two-phase bearingless slice motors," *IEEE Trans. Ind. Electron.*, vol. 58, no. 5, pp. 1921–1925, May 2011.

[8] A. K. Morya, M. C. Gardner, B. Anvari, L. Liu, A. G. Yepes, J. Doval-Gandoy, and H. A. Toliyat, "Wide bandgap devices in AC electric drives: Opportunities and challenges," *IEEE Trans. Transport. Electrif.*, vol. 5, no. 1, pp. 3–20, March 2019.

[9] D. Jang, "PWM methods for two-phase inverters," *IEEE Ind. Appl. Mag.*, vol. 13, no. 2, pp. 50–61, 2007.

[10] S. Ziaeinejad, Y. Sangsefidi, H. Pairodin Nabi, and A. Shoulaie, "Direct torque control of two-phase induction and synchronous motors," *IEEE Trans. Power Electron.*, vol. 28, no. 8, pp. 4041–4050, 2013.

[11] E. Gurpinar, A. Castellazzi, F. Iannuzzo, Y. Yang, and F. Blaabjerg, "Ultra-low inductance design for a gan hemt based 3l-anpc inverter," in *Proc. IEEE Energy Convers. Congr. and Expo. (ECCE)*, 2016, pp. 1–8.

[12] M. S. Islam, R. Mikail, and I. Husain, "Slotless lightweight motor for aerial applications," *IEEE Trans. Ind. Appl.*, vol. 55, no. 6, pp. 5789–5799, 2019.

[13] X. Liu, A. M. Cramer, V. Rallabandi, and D. M. Ionel, "Switching frequency selection for ultra-low-inductance machines," in *Proc. IEEE Int. Electr. Mach. Drives Conf. (IEMDC)*, May 2017, pp. 1–6.